Eur. Phys. J. D **19**, 245–255 (2002)
DOI: 10.1140/epjd/e20020075

THE EUROPEAN PHYSICAL JOURNAL D
EDP Sciences

Onset of instabilities in self-pulsing semiconductor lasers with delayed feedback

T.W. Carr[a]

Department of Mathematics, Southern Methodist University, Dallas, Texas 75275-0156, USA

Received 1st August 2001 and Received in final form 28 November 2001

Abstract. We consider the deterministic dynamics of a semiconductor laser with saturable absorber that is subject to delayed optical feedback. Alone, both the saturable absorber and delayed feedback cause the CW output to become unstable to periodic output *via* Hopf bifurcations. We examine the combined effects of these two destabilizing mechanisms to determine new conditions for the Hopf bifurcations. We also describe the transient as the unstable CW output evolves to the oscillatory state. A main result is that the presence of a saturable absorber can increase the sensitivity of the laser to delayed feedback.

PACS. 05.45.-a Nonlinear dynamics and nonlinear dynamical systems – 42.55.Ah General laser theory – 42.55.Px Semiconductor lasers; laser diodes

1 Introduction

Lasers with an intracavity saturable absorber (LSA) have long been used to generate high-intensity pulses (see [1,2] for background and historical references). The effect of the absorber is to passively modulate the cavity losses so that the LSA is "self-pulsing." The pulsed output is of practical interest for applications that require extremely short high-peak-power pulses of light. Self-pulsing semiconductor lasers (SPSL) exhibit a high repetition rate that ranges from hundreds of megahertz to a few gigahertz [3]. They are interesting for telecommunication and for optical data storage using compact disc (CD) or digital versatile disc (DVD) systems [4,5].

Delayed-optical feedback can result from reflections off an external surface. Delayed feedback in semiconductor lasers has been successfully used for linewidth narrowing and mode selection [3]. However, the stability of the semiconductor laser's CW output has been shown to be very sensitive to delayed optical feedback. Lang and Kobayashi [6] provided a theoretical description in the form of rate equations to describe the destabilizing effect of feedback on the laser's CW output. Since then a large body of work has developed investigating the onset of instabilities and the progression to chaotic output referred to as "coherence collapse" (see [7] for a review). More recently, the phenomenon of LFF, or "Low-Frequency Fluctuations", which are recurrent deep drops in the laser's intensity, has been actively investigated (see [8] and included references).

Part of the success in using for SPSLs in CD and DVD systems is due to the fact that the self-pulsations reduce feedback-induced noise [9–11]. More recently, van Tartwijk and San Miguel [12] have numerically investigated the effect of delayed feedback in SPSLs to better quantify the statistical properties of the pulse amplitude and repetition rate due to stochastic noise. However, an analysis of the combined deterministic dynamics of the SPSL and delayed-optical feedback, to our knowledge, has not been reported. In the present paper we report our first results in this effort.

In this paper, we determine the conditions for the onset of oscillations and pulsations due to the presence of a saturable absorber (SA) and delay-feedback (DF). Individually, both the SA and DF cause the laser's CW output to become unstable through Hopf bifurcations. Our instability result is expressed in terms of deviations from the conditions describing only the sole effect of either the SA or DF. We use numerical simulation of rate-equations to verify our results as well as to describe the transient dynamics as the instabilities develop.

We consider a modification of the well-known Lang-Kobayashi [6] equations for semiconductor lasers subject to delayed feedback with the additional effect of nonlinear loss due to the saturable absorber. In Appendix A we show how (1) is derived as a nondimensional version of the model used by van Tartwijk and San Miguel [12]. We have

$$\begin{aligned}\frac{\mathrm{d}E}{\mathrm{d}t} &= \frac{1}{2}[(1+\mathrm{i}\alpha)D_1 + (1+\mathrm{i}\alpha)\frac{A_2}{1+a|E|^2} - 1]E \\ &\quad +\eta\exp(-\mathrm{i}\omega_\eta\tau)E(t-\tau), \\ \frac{\mathrm{d}D}{\mathrm{d}t} &= \gamma[A_1 - (1+|E|^2)D], \end{aligned} \tag{1}$$

[a] e-mail: tcarr@mail.smu.edu

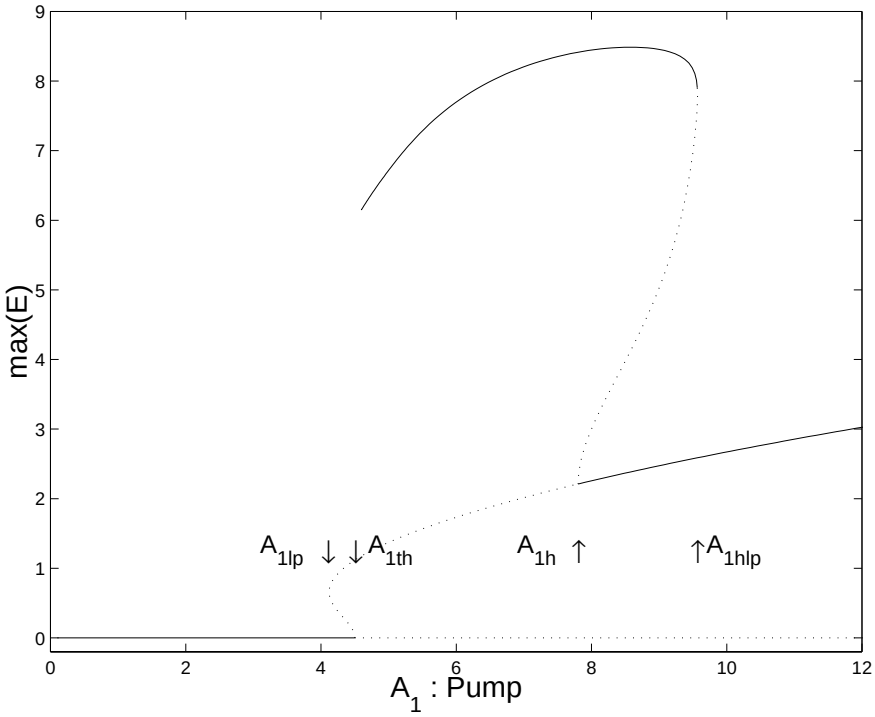

Fig. 1. Bifurcation diagram [29] of the LSA without feedback ($\eta = 0$). Solid/dotted lines are stable/unstable solutions, respectively. $A_{1\mathrm{th}} = 4.5$ is the bifurcation of the zero steady state to the non-zero steady state. $A_{1\mathrm{lp}} = 4.1$. $A_{1\mathrm{h}} = 7.8$ is the Hopf bifurcation to periodic solutions that are unstable. Pulsating solutions occur on the upper branch between $A_{1\mathrm{hlp}} = 9.6$ and $A_{1\mathrm{th}}$, where they terminate in a homoclinic orbit ($A_2 = -3.5$, $a = 2$, $\gamma = 0.05$).

where E is the electric field and D is the population inversion. The parameter γ is the inversion-decay rate normalized by the cavity-decay rate and A_1 is due to the pump (or injected current in the case of semiconductor lasers). $A_2 < 0$ is defined as the absorber-pump parameter and a describes the relative saturability of the absorber with respect to the active media. The linewidth enhancement factor α is assumed to be equal for both the active and absorbing material. The feedback strength is given by η and delay by τ, while ω_η in the feedback phase is the frequency of the solitary laser.

In previous work we documented the nondimensionalized parameter values for various semiconductor lasers [13]. The range of values of these parameters may depend on the type of laser, but they all exhibit small values of γ ($O(10^{-3})$); the strongly pulsating behavior of the LSA is directly related to the small values of γ [14]. For self-pulsing semiconductor lasers, (1) can be supplemented by additional terms modeling nonlinear gain saturation, nonlinear damping of the active and passive regions and cross-diffusion of the carriers between active and passive regions. However, none of these additional effects is responsible for the generation of self-pulsation and none leads to qualitatively different dynamics [13].

Self-pulsation of the LSA without feedback ($\eta = 0$) appears through a bifurcation mechanism that we briefly review for the case shown in Figure 1. The laser-first threshold occurs when $A_1 = A_{1\mathrm{th}} \equiv 1 - A_2$, and the non-zero steady state (NZSS) may appear through either a supercritical or subcritical bifurcation. In Figure 1 we show the bifurcation diagram for the subcritical case. A Hopf bifurcation to pulsating solutions appear on the non-zero branch of solutions at $A_{1\mathrm{h}}$ and is subcritical so that the oscillatory solutions are unstable. The oscillations become stable pulsations as the branch passes the turning point at $A_{1\mathrm{hlp}}$. As A_1 is decreased the oscillations become increasingly pulsating with increasing interpulse periods. The branch terminates at a homoclinic orbit of infinite period as A_1 approaches $A_{1\mathrm{th}}$. We note that the unstable branch of oscillatory solutions serves as a basin boundary between the NZSS and the pulsating solutions for $A_{1\mathrm{h}} < A_1 < A_{1\mathrm{hlp}}$.

In the next section we determine the steady-state solution of (1) when there is feedback ($\eta \neq 0$). We then determine the conditions for a Hopf bifurcation and discuss how they differ from the cases of SA without DF or DF without the SA. In Section 4 we find an approximation to the harmonic solutions that appear as the feedback is increased. In Section 3 we use numerical simulation to demonstrate our results, followed by a discussion in Section 5.

2 Hopf-bifurcation conditions

To determine the new NZSS in the presence of feedback, let $E(t) = F(t)\exp[\mathrm{i}\Phi(t) - \omega_\eta t]$ in (1):

$$\begin{aligned}
\frac{\mathrm{d}F}{\mathrm{d}t} &= \frac{1}{2}\left[D + \frac{A_2}{1+aF^2} - 1\right]F(t) \\
&\quad +\eta F(t-\tau)\cos[\Phi(t-\tau) - \Phi(t)], \\
\frac{\mathrm{d}\Phi}{\mathrm{d}t} &= \omega_\eta + \frac{\alpha}{2}\left[D + \frac{A_2}{1+aF^2}\right] \\
&\quad +\eta\frac{F(t-\tau)}{F(t)}\sin[\Phi(t-\tau) - \Phi(t)], \\
\frac{\mathrm{d}D}{\mathrm{d}t} &= \gamma[A_1 - (1+F^2)D]. \qquad (2)
\end{aligned}$$

We look for steady-state solutions by setting $[F(t), \Phi(t), D(t)] = (F_\mathrm{s}, \omega_\mathrm{s} t, D_\mathrm{s})$. The zero-intensity steady state is $(F_\mathrm{s}, D_\mathrm{s}) = (0, A_1)$. When the laser is at steady state, the effect of the feedback is constant, *i.e.*, $F(t-\tau) = F_\mathrm{s}$ and $\cos[\Phi(t-\tau) - \Phi(t)] = \cos(\omega_\mathrm{s}\tau)$. Thus the NZSS will be shifted by an $O(\eta)$ amount. When the pump is increased the zero-intensity steady state becomes unstable at a value of A_1 near $A_{1\mathrm{th}}$ that we determine below. The new NZSS is defined by the bifurcation equation relating the intensity $I = F_\mathrm{s}^2$ to the pump:

$$A_1 = (1+I)\left[1 - \frac{A_2}{1+aI} - 2\eta\cos(\omega_\mathrm{s}\tau)\right],$$

$$D_\mathrm{s} = \frac{A_1}{1+I}, \tag{3}$$

$$\omega_\mathrm{s} = (\omega_\eta + \frac{\alpha}{2}) - \eta\sqrt{1+\alpha^2}\sin(\omega_\mathrm{s}\tau + \arctan\alpha). \tag{4}$$

The frequency of the electric field ω_s is given by the transcendental equation (4) and has multiple solutions depending on the value of η; initial conditions and stability conditions generally determine which solution is selected [15] in the deterministic case. The value of the pump at the bifurcation point can be found by taking $I = 0$:

$$A_1 = A_{1\mathrm{th}} - 2\eta\cos(\omega_\mathrm{s}\tau). \tag{5}$$

The bifurcation to the NZSS may be supercritical or subcritical depending on a and A_2. It is subcritical and has a limit point if there is a value of $I = I_\mathrm{lp}$ such that $\mathrm{d}A_1/\mathrm{d}I = 0$ and $I_\mathrm{lp} > 0$. We find that

$$I_\mathrm{lp} = -\frac{(a-1)A_2 + 1 - 2\eta\cos(\omega_\mathrm{s}\tau)}{a[1 - 2\eta\cos(\omega_\mathrm{s}\tau)]}\,. \tag{6}$$

The value of the pump at the limit point can be found be substituting I_lp into the bifurcation equation (3). In Figure 1 we show the complete bifurcation diagram, steady states and periodic solutions for the LSA without feedback. When $\eta = 0$ the zero steady state bifurcates to the NZSS when $A_1 = A_{1\mathrm{th}}$. As described above, feedback will shift $A_{1\mathrm{th}}$ and $A_{1\mathrm{lp}}$ by an $O(\eta)$ amount.

The stability of the NZSS is investigated by substituting $(F, \Phi, D) = (F_\mathrm{s}, \omega_\mathrm{s} t, D_\mathrm{s}) + (u, \phi, v)$ into (2) and examining the time evolution of the small perturbations (u, ϕ, v). The resulting equations for (u, ϕ, v) are linearized for $(u, \phi, v) \ll 1$. The conditions for a Hopf bifurcation are determined by looking for solutions proportional to $\exp(\mathrm{i}\omega t)$ and setting the determinant to zero. The real and imaginary parts of the determinant give two conditions for the Hopf frequency ω and the value of the intensity $I = F_\mathrm{s}^2$ at the Hopf bifurcation point. The value of the pump at the Hopf bifurcation point A_1 is determine by I using the bifurcation equation (3). When there is no feedback ($\eta = 0$) the conditions for the LSA are relatively simple; we state these here for reference:

$$\gamma(1+I)(1+aI)^2 + aA_2 I = 0,$$

$$\omega^2 = \frac{\gamma I}{(1+aI)^2}[(1+aI)^2 + (a-1)A_2]. \tag{7}$$

For $\gamma \ll 1$ the leading-order approximation for the intensity at the Hopf bifurcation is $I^2 = -A_2/(\gamma a)$ and the Hopf frequency is $\omega^2 = \gamma I$. The leading-order approximation for the Hopf frequency is identical to the relaxation frequency of the solitary laser without DF or SA.

The general case of the LSA with feedback ($\eta \neq 0$) produces a much more complicated result, which is given in Appendix B. Similar equations have been derived for the Lang-Kobayashi model without the effects of the SA by Erneux [16]. The inclusion of the SA makes both analytical and numerical analysis of these equations difficult. However, we can gain further information by examining specific limits. We shall focus on the most generic case, avoiding the special cases of short delay or large feedback.

We examine the Hopf conditions using the scalings $I = F_\mathrm{s}^2 = O(\gamma^{-1/2})$, $\omega = O(\gamma^{1/4})$, and $\eta = O(\gamma^{1/2})$; these scalings are motivated by conditions (7). To leading order we find that,

$$\omega = \gamma^{1/2}\sqrt{I} + O(\gamma^{1/2}), \tag{8}$$

and

$$\eta = -\frac{\gamma I^2 + A_2/a}{I2\sin^2(\omega\tau/2)[\cos(\omega_\mathrm{s}\tau) + \alpha\sin(\omega_\mathrm{s}\tau)]} + O(\gamma^{3/4}), \tag{9}$$

where we have recovered the scaling parameter γ into the result. The value of the pump A_1 where the Hopf bifurcation occurred can be found by applying the above scalings along with $A_1 = O(\gamma^{-1/2})$ to the bifurcation equation (3). Similar results have been found for the case of semiconductor lasers without saturable absorbers [15,17], where here the pump is replaced by the deviation from the LSA Hopf-bifurcation point. Specifically, if there is no feedback, $\eta = 0$, the value of the intensity where the Hopf bifurcation occurs is $I_0^2 = |A_2|/\gamma a$ (this is the leading-order approximation to the upper Hopf-bifurcation point for the LSA). We then define $\eta_0 = \eta\,(A_2 = 0)$ as the Hopf-bifurcation point in the absence of the saturable absorber. With these definitions we may express the combined effect of the feedback and SA as

$$\frac{\eta}{\eta_0} = \frac{I^2 - I_0^2}{I^2}\,. \tag{10}$$

The Hopf conditions (9) and (10) indicate that the diode-LSA is more sensitive to feedback than a diode-laser without a saturable absorber. For all values of the intensity I, $\eta/\eta_0 < 1$. The Hopf bifurcation occurs at values of η less than that when there is no saturable absorption. Indeed, close to the original LSA Hopf-bifurcation point, where $I \approx I_0^2$, only small amounts of feedback will lead to oscillations. We will return to this point later.

The leading order Hopf conditions (9) and (10) are somewhat crude for quantitative comparison with the full problem. Equation (9) predicts branches of solutions with well-defined minimums separated by the singularities when $\sin(\omega\tau/2) = 0$. These features are difficult to identify in simulations of (1). However, we find that

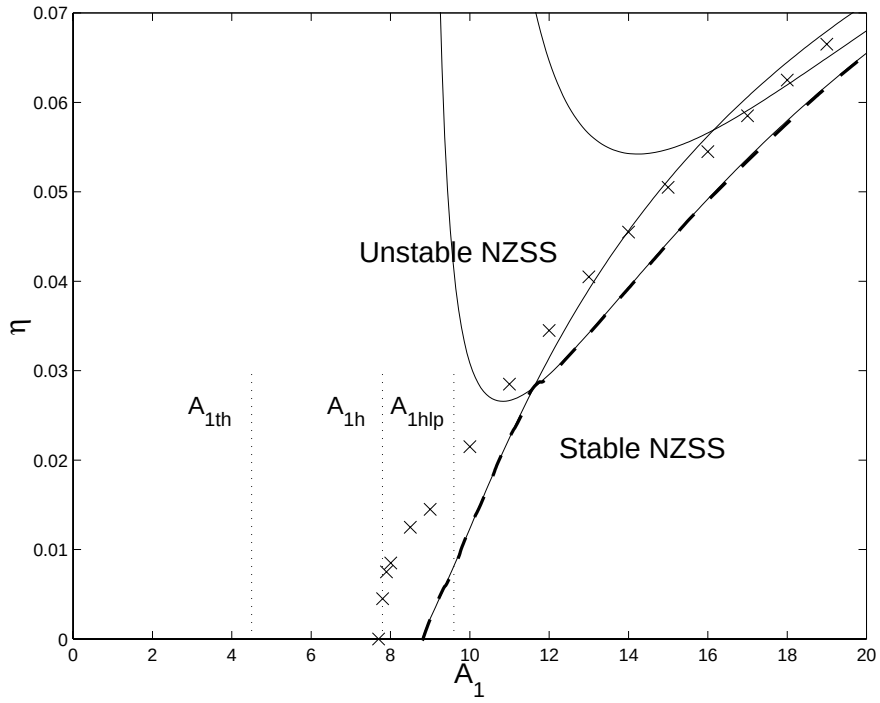

Fig. 2. Solid lines: linear-stability condition (11) with parameter values the same as in Figure 1. For a fixed value of A_1 the envelope of the curves, highlighted with a thick dash line, determines the feedback level for a Hopf bifurcation. The crosses ($\times$) are the Hopf bifurcation points determined by direct simulation of (1).

a higher-order approximation, which we can solve numerically, produces excellent results. Using the same scalings as above we consider the two conditions

$$\eta G_1(\gamma DI - 2\omega^2\cos(\omega_s\tau)) + \omega^2\left(\gamma I + \frac{A_2}{aI}\right) + O(\gamma) = 0,$$

$$\omega^3 - \omega\gamma I + \eta G_2(\gamma ID - 2\omega^2\cos(\omega_s\tau)) + O(\gamma^{5/4}) = 0, \tag{11}$$

where D and G_j depend on ω_s and ω, and are defined in Appendix B. Along with the steady-state equation (4) this defines three equations for ω, I, and ω_s. Subsequently, we will confine our analysis to the "minimum-linewidth mode" [7,15] when $\omega_s\tau = -\arctan(\alpha)$ and analyze equations (11). Lastly, we mention that the numerical results from equations (11) very accurately describe those of the full problem equation (9), while at the same time allow for easy identification of the dominant terms.

In Figure 2 we show the multiple solutions of (11) as a function of the pump A_1 and the feedback η. The envelope of the multiple solutions defines the primary-Hopf bifurcation, emphasize by the thick-dashed line in Figure 2, and separate stable and unstable parameter regimes. For fixed pump A_1, if the feedback is increased above the value defined by the envelope, the NZSS becomes unstable. If there is no feedback, $\eta = 0$, the SA still causes a Hopf bifurcation point that is indicated by the principal curve emerging from $\eta = 0$. Due to the saturable absorber, there is a large overlap of the multiple solutions so that the distinct minimums of the stability curves can not be differentiated. As the pump is increased beyond the primary-Hopf bifurcation envelope, the overlapping multiple solutions lead to Torus bifurcations and other complex phenomena, which are a generic phenomena of semiconductor lasers with DF [16,18].

The analytical results are confirmed by direct numerical simulation of the full equations using the *Matlab routine dde23* [19]. The results are shown in Figure 2 by the crosses ($\times$) that indicate the primary-Hopf bifurcation for a given value of the pump. For each value of the pump A_1 we increased the feedback η until perturbations to the system became unstable; our results are accurate to $\eta = \pm 0.0005$. The shift in the Hopf bifurcation close to A_{1h} between the numerical results and that predicted by (11) is reasonable for the value of γ used. As the pump is increased the numerical simulations confirm that the multiple solutions cannot be differentiated.

Figure 3a shows the case of the semiconductor laser with an extremely weak SA, $A_2/a \ll 1$. The dotted line reproduces the result of Figure 2. For a fixed value of the pump, A_1, the dotted curves ($A_2/a = O(1)$) are crossed much sooner than the solid curves ($A_2/a \ll 1$); the saturable absorber reduces the necessary level of feedback for instability. It should be noted that if $A_2/a = 0$, then the Hopf bifurcation is singular as $A_1 \to A_{1th}^+$. There will not be an instability curve continuing all the way to $\eta = 0$ because without SA and DF the solitary laser does not have a Hopf bifurcation. We have kept $A_2/a \neq 0$ for more direct comparison with the $A_2/a = O(1)$ case.

The parameters γ and τ are modified in Figures 3b and 3c, respectively. In Figure 3b γ is reduced, shifting the curves to the right, because $A_{1h} = O(\gamma^{-1/4})$. In Figure 3c, the delay time τ has been increased, producing a smooth envelope of curves that determines the Hopf-bifurcation point. Other than shifting the bifurcation curves or

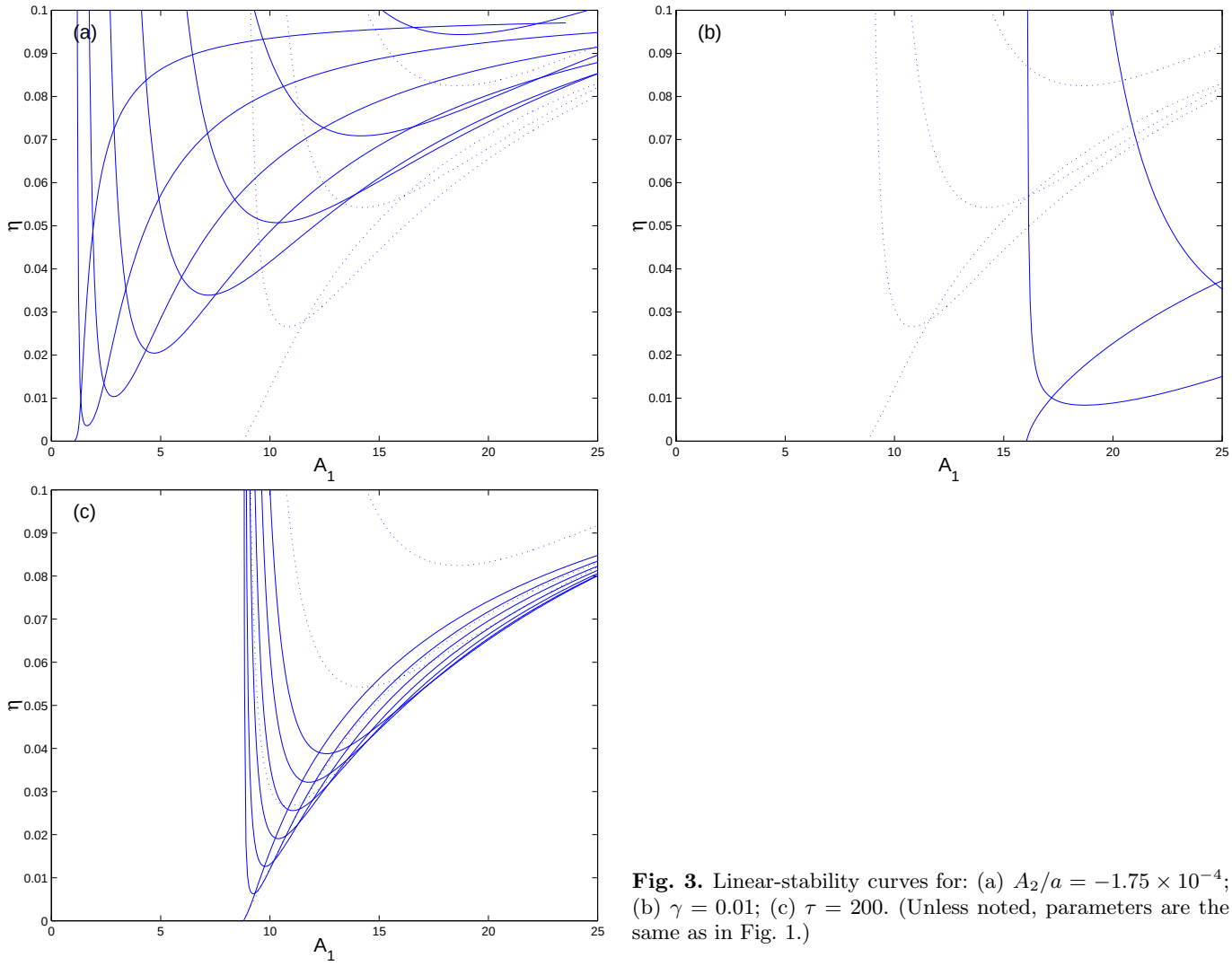

Fig. 3. Linear-stability curves for: (a) $A_2/a = -1.75 \times 10^{-4}$; (b) $\gamma = 0.01$; (c) $\tau = 200$. (Unless noted, parameters are the same as in Fig. 1.)

contracting/expanding the space between them, the behavior of the system remains the same.

3 Transient response to feedback

In the previous section, we determined the parameter conditions that lead to instabilities due to the presence of feedback. In the present section we analyze the transient response leading to either pulsations or complex oscillations upon the initiation of feedback. Here we will concentrate on when $A_1 > A_{1\mathrm{h}}$, when there is either bistability, or $A_{1\mathrm{h}} < A_1 < A_{1\mathrm{hlp}}$, when there is only the NZSS. We have used the *Matlab routine dde23* [19] for our numerical simulations. We have also confirmed that our results using *dde23* [19] without feedback are consistent with higher-order numerical methods such as the *Matlab routine ode45*.

We first tune the laser very near the LSA Hopf-bifurcation point $A_{1\mathrm{h}}$. In Figure 4a $A_1 = 8.0$ and small feedback, turned on when $t = 200$, leads to harmonic solutions. The harmonic solutions can be described by a weakly nonlinear analysis that is presented in the next section. However, for slightly larger feedback in Figure 4b, as the oscillations grow they collide with the branch of unstable periodic orbits related to the LSA's unstable branch of solutions. Subsequently, the trajectory of solutions falls into the basin of self-pulsing solutions that quickly develop.

The scenario is qualitatively similar for larger values of the pump as shown in Figure 5b when $A_1 = 8.5$. However, in this case much larger feedback is required to initiate self-pulsations. This is because as A_1 is increased the basin for the NZSS increases relative to the basin for the self-pulsing solutions in Figure 1. In Figure 5c, the saturable absorber is removed by setting $A_2 = 0$. Now the only cause of instability is the DF, so there may be complex oscillations but not the self-pulsing solutions due to the SA.

Finally, in Figure 6, $A_1 > A_{1\mathrm{hlp}}$ so that the laser is outside the domain of self-pulsations. Here, large feedback leads to complex oscillations typical of semiconductors with DF.

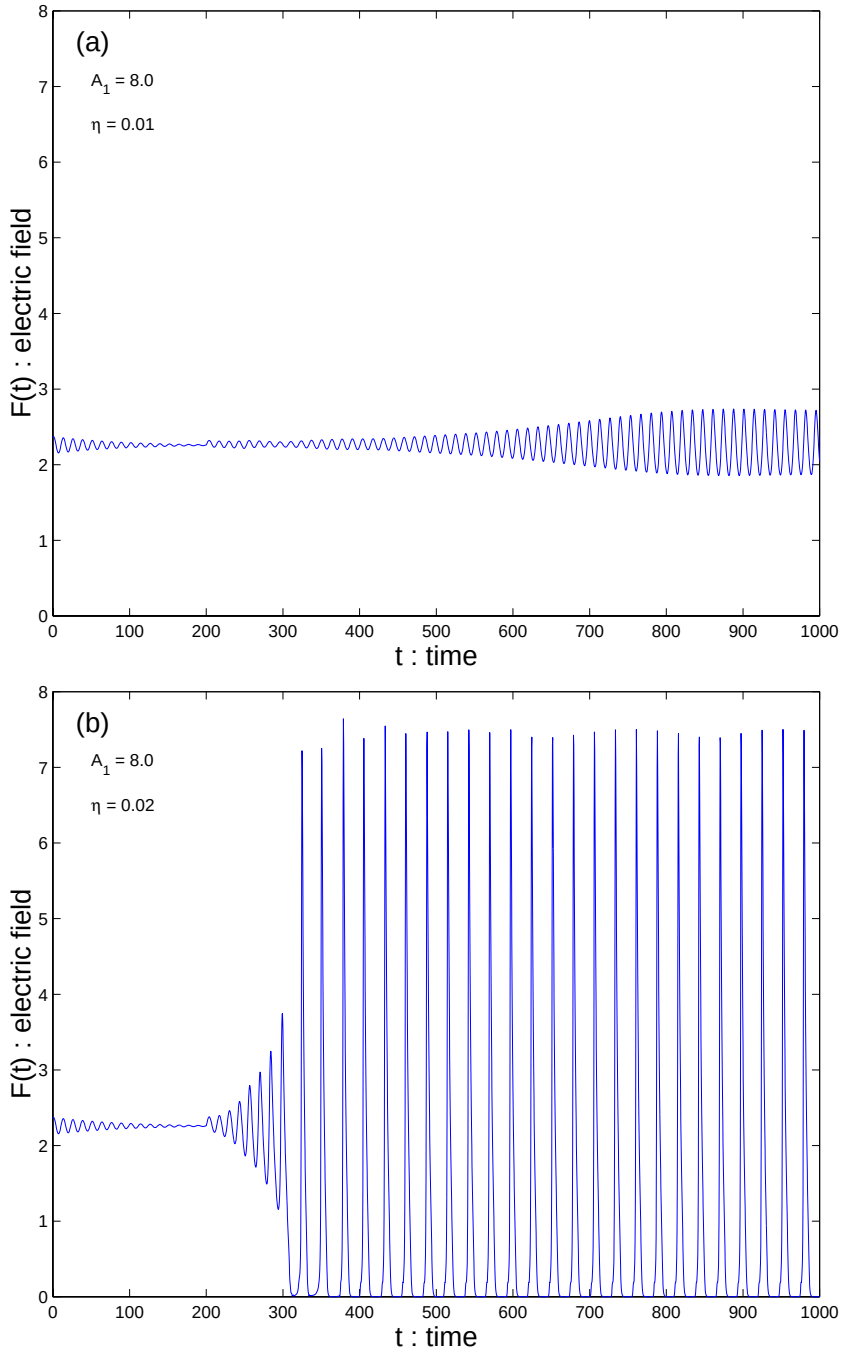

Fig. 4. $A_1 = 8.0$, and (a) $\eta = 0.01$, (b) $\eta = 0.02$. The feedback is initially off ($\eta = 0$) and then turned when $t = 200$. Near the Hopf-bifurcation point ($A_{1h} = 7.8$) small feedback causes harmonic solutions, while larger feedback causes pulsating solutions. Feedback is turned on at $t = 200$ and, unless noted, parameters are the same as in Figure 1.

4 Harmonic solutions

So far our analysis has concentrated on the linear stability of the NZSS and the evolution to either pulsating or harmonic solutions. The purpose of the present section is to formulate a nonlinear theory for the resulting oscillations. Previously, an asymptotic analysis based on the limits γ, $\eta \ll 1$ and $\alpha \gg 1$ has been successfully used to analyze semiconductor lasers subject to delayed feedback and injection [20–22], as well as arrays of coupled semiconductor lasers [23], and a multimode semiconductor laser [24]. The qualitative results for large α have shown excellent qualitative agreement with numerical and experimental results for more realistic values of ($\alpha \approx 5$). We have applied a similar analysis to equation (2) and because the asymptotic method has been well documented in the above references, we quote only our bifurcation result.

We look for solutions of the form

$$F = \sqrt{I}\left(1 + \frac{y}{\alpha}\right) e^{i\Phi}, \quad D = \frac{A_1}{1+I}\left(1 + 2\frac{\omega}{\alpha}x\right), \qquad (12)$$

where (x, y) are deviations from the steady-state solutions. We find that to leading order

$$x(t) = -B\sin(\omega t + \psi), \quad y(t) = -B\cos(\omega t + \psi),$$
$$\Phi(t) = B\cos(\omega t + \psi) + \phi. \qquad (13)$$

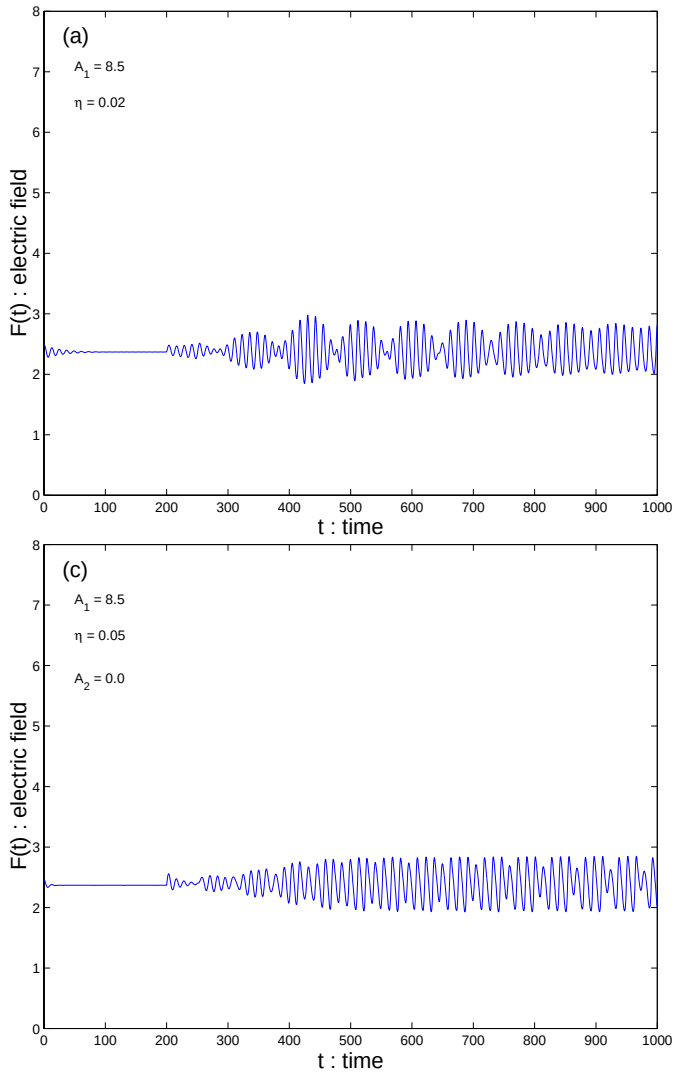

Fig. 5. $A_1 = 8.5$, and (a) $\eta = 0.02$, (b) $\eta = 0.05$. Away from the Hopf bifurcation larger feedback is needed to cause either harmonic or pulsating solutions. In (c) $\eta = 0.05$ (same as (b)) but $A_2 = 0$ so that there is no saturable absorber. The feedback is large enough to cause an instability, but pulsating solutions are not possible. (Feedback is turned on at $t = 200$ and, unless noted, parameters are the same as in Fig. 1.)

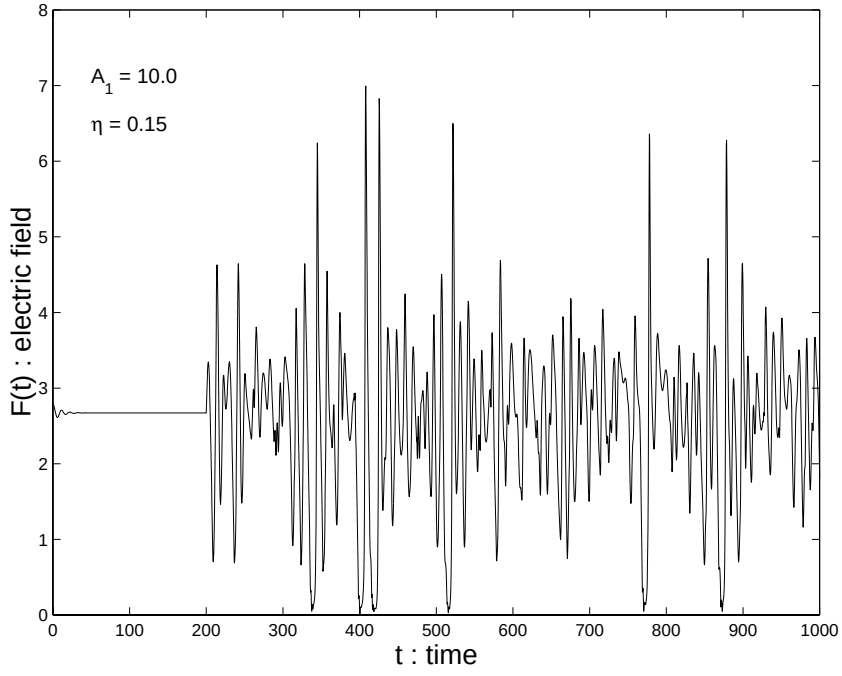

Fig. 6. $A_1 = 10.0$, and $\eta = 0.15$. For $A_1 > A_{1\mathrm{hlp}}$, very large feedback induces not pulsations, but complex dynamics similar to to semiconductors without the saturable absorber. (Feedback is turned on at $t = 200$ and, unless noted, parameters are the same as in Fig. 1.)

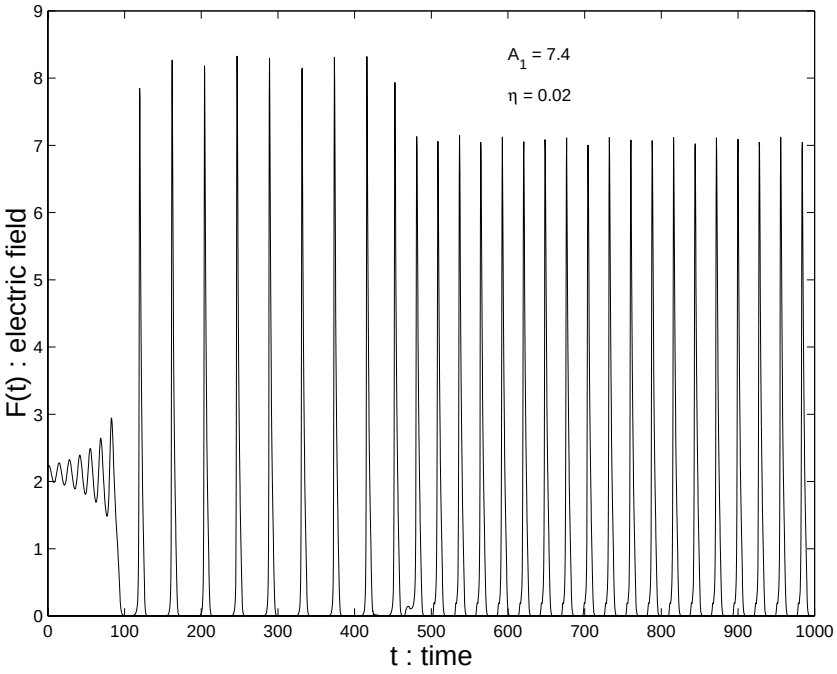

Fig. 7. $A_1 = 7.4$, and $\eta = 0.02$. Effect of feedback turned on at $t = 400$ on saturable absorber-induced pulsations. (Unless noted, parameters are the same as in Fig. 1.)

The phase variables ψ and ϕ are slowly evolving but are not necessary for the present analysis. For the amplitude B we obtain the bifurcation equation

$$\eta = -\frac{\gamma I^2 + A_2/a}{\alpha I 2 \sin(\omega\tau/2)\sin(\omega_s\tau)} \frac{B}{J_1(2B\sin(\omega/\tau/2))}, \quad (14)$$

where ω is the approximate Hopf-bifurcation frequency given by (8) and $J_1(x)$ is the order-1 Bessel function of the first kind. The steady-state frequency ω_s is given by the leading-order approximation to (4) as

$$\omega_s = \omega_\eta + \frac{\alpha}{2} + O(\eta). \quad (15)$$

As the amplitude B goes to zero we recover the $\alpha \gg 1$ version of the linear-stability result (9) that predicts the bifurcation point.

The bifurcation equation (14) is analogous to equation (3.12) in Alsing *et al.* [20]. For a fixed steady-state intensity greater than the Hopf-bifurcation point ($\gamma I^2 + A_2/a > 0$), as the feedback η is increased, there is a supercritical bifurcation to oscillatory solutions described by (12). For large values of feedback, saddle-node bifurcations to higher-amplitude solutions coexist with the original bifurcating solution. Thus, the bifurcation equation (14) predicts that the SPSL with DF operates like semiconductor laser with DF whose linear dissipation is controlled by the distance from the upper Hopf-bifurcation point ($\gamma I^2 + A_2/a > 0$). The analysis assumes small-amplitude solutions; thus, the conclusion is not valid for values of A_1 and η, where self-pulsations will develop.

Our analysis accounts for the nonlinear effects of the DF, while the SA contributes as a linear dissipation term. Indeed, without DF, the equation is singular and cannot describe the bifurcation due to the SA alone. To simultaneously capture the nonlinear effects of both the DF and the SA requires continuing the analysis to $O(1/\alpha^2)$. However, such an analysis is analytically intractable. Similarly, without DF ($\eta = 0$), the nonlinear effect of the saturable absorber is a subcritical-Hopf bifurcation, as shown in Figure 1. The SA bifurcation without DF can be described by a weakly nonlinear analysis and the derivation of an evolution equation. Again, as in the previous case, the nonlinear contributions of the SA and DF appear at different orders of the perturbation analysis such that it is very difficult to simultaneously capture their nonlinear effects.

5 Discussion

Semiconductor lasers with feedback display numerous bifurcations, multistability, LFF, and chaos as the feedback is increased. We have considered weak feedback, avoiding complex phenomena, to focus on the interaction with a saturable absorber. Also, we focused on the initial bifurcation from the NZSS and the resulting evolution to oscillations, whether harmonic, complex or pulsing. We have not discussed the asymptotic effect of feedback on the self-pulsing solutions when $A_{1\mathrm{th}} < A_1 < A_{1\mathrm{hlp}}$, which can be significant. In Figure 7 we show pulsations due to the saturable absorber both before and after the application of feedback. The feedback affects both the amplitude and the period of the pulsations (see also Fig. 12 in [12]), which are critical design parameters in devices. A detailed analysis to quantify these effects is underway.

We mention that we have used the laser with SA (no DF) as a reference for critical points such as $A_{1\mathrm{h}}$ and

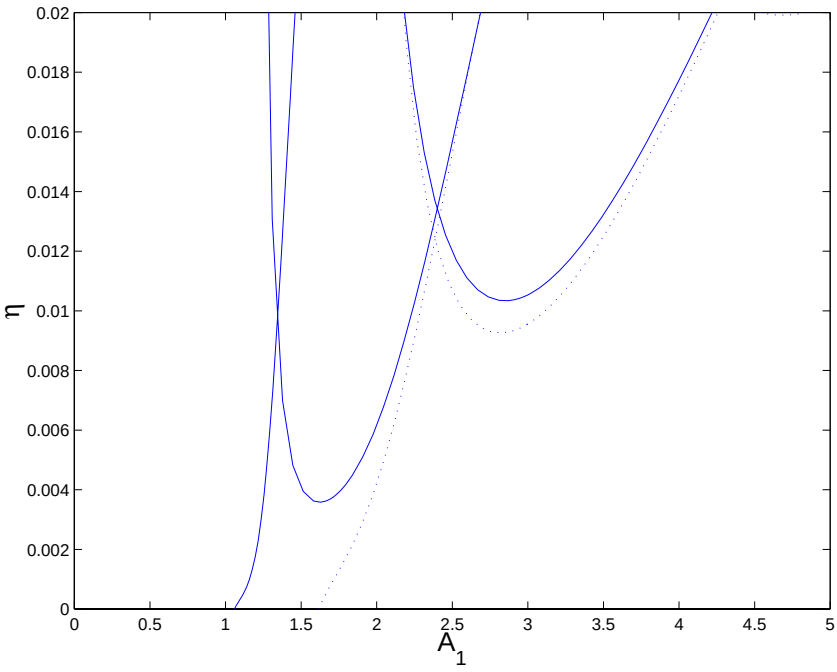

Fig. 8. Semiconductor laser with delayed feedback and no saturable absorber $A_2 \approx 0$ (solid curve), and very weak saturable absorber $A_2 = -0.035$ (dotted curve).

$A_{1\mathrm{hlp}}$ (see Fig. 1). However, these are shifted by only a small amount, $O(\eta)$, when weak DF is present.

Our reference value of the nondimensional delay time was $\tau = 50$, which corresponds to an external cavity length of $L_{\mathrm{ext}} = 2$ cm ($\tau = 2L_{\mathrm{ext}}\Gamma_0/c$, where c is the speed of light and from [12] we use $\Gamma_0 = 0.367$ (ps)$^{-1}$). As the cavity length is increased, Figure 3c shows that the envelope of the family of neutral stability curves determines the effective Hopf-bifurcation point. For short external cavities, further analytical approximations are possible [16,25,26]. We observe from our numerical analysis of (11) that the multiple neutral-stability curves spread in A_1 and increase in η. The Hopf-bifurcation point is determined solely by the primary curve emanating from $\eta = 0$.

For numerical convenience we have used a larger than normal value for the decay rate $\gamma = O(10^{-2})$ in our simulations; for semiconductor lasers, γ is typically $O(10^{-3})$. Our choice dramatically improves the accuracy as well as the speed of the simulations, because the period of the self-pulsing solutions scales as $O(\gamma^{-1/4})$. Our results are not changed for smaller γ and all conclusions remain qualitatively valid (see Fig. 3b).

A main result of our analysis is the prediction that the saturable absorber increases the sensitivity of the semiconductor laser to feedback from the point of view of the onset of oscillations; this is in contrast to the regime of self-pulsations for $A_{1\mathrm{th}} < A < A_{1\mathrm{hlp}}$, whose noise-sensitivity may be reduced by feedback [12]. To elucidate this point we consider the case of "parasitic" saturable absorption. The linear-stability results for this case are shown in Figure 8. The solid curve is the prediction of the Hopf bifurcation due to feedback when $A_2 \ll 1$ in (11) and shown in Figure 3a. The dotted curve is for $A_2 = -0.035$, which is one hundred times smaller than typical values. The first threshold, $A_{1\mathrm{th}} = 1 - A_2$, will shift only a small amount. However, an $O(1)$ interval of self-pulsations will appear because $A_{1\mathrm{h}} = O(\gamma^{-1/4})$. To avoid the self-pulsing regime the laser is tuned outside this interval, where the difference between the curves shows the increased sensitivity to feedback.

Also interesting is the case of a weak SA defined by $a \ll 1$, which indicates that the absorber requires very intense fields to saturate. For small a the typical bifurcation scenario is different than depicted by Figure 1. Instead, the NZSS appears through a forward/supercritical bifurcation, and there are lower and upper Hopf bifurcations connecting a branch of periodic solutions (see Fig. 2 in [27]). As the pump is increased, the zero stead-state losses stability to CW output. We would like to know what is the combined effect of DF and the SA as the pump is increased, and the laser nears the lower Hopf bifurcation point. We have reanalyzed the linear stability conditions for the case of $a = O(\gamma)$. Without feedback, the Hopf bifurcation occurs when $I = I_0 = 1/[(a/\gamma)|A_2| - 1]$. Positivity determines a minimum value of A_2, which indicates that for a weak SA the absorber requires a minimum amount of reverse pump to induce oscillations. The effect of DF without the SA is given by η_0 as in (10). Then for DF with a weak SA we have

$$\frac{\eta}{\eta_0} = \frac{1}{I} - \frac{1}{I_0}, \quad I \leq I_0. \tag{16}$$

The condition $I \leq I_0$ is required because we are increasing the pump A_1, hence I, until the lower Hopf bifurcation is reached at I_0. There is a critical value $I_{\mathrm{c}} \equiv I_0/(1 + I_0)$ where $\eta/\eta_0 = 1$. For $I < I_{\mathrm{c}}$, $\eta/\eta_0 > 1$, indicating that the weak SA is strongly dissipative and more than normal DF is required to induce oscillations. This is because the field is too weak for the saturation term to have an effect. For $I > I_{\mathrm{c}}$, $\eta/\eta_0 < 1$, indicating that the weak SA is again causing increased sensitivity to DF.

The high-intensity Hopf bifurcation at $A_{1\mathrm{h}}$ may be supercritical for some parameter values. In this case $A > A_{1\mathrm{h}}$ is outside the domain of self-pulsing solutions. However, our results for the bifurcation point (9) and the bifurcation equation (3) are still valid. In this regime, the SA will increase the sensitivity to DF as described above.

The author would like to thank Larry Shampine, Skip Thompson, and Didier Pieroux for useful discussions concerning the numerical solution of DDEs. This work was supported by the National Science Foundation Grant No. DMS-9803207.

Appendix A: Derivation of model

Van Tartwijk and San Miguel [12] proposed the following model for the LSA subject to delayed feedback:

$$\begin{aligned}\frac{\mathrm{d}E}{\mathrm{d}t} &= \frac{1}{2}[(1+\mathrm{i}\alpha)\Gamma_1\xi_1(N_1-N_{t1}) \\ &\quad +(1+\mathrm{i}\alpha)\Gamma_2\xi_2(N_2-N_{t2})-\Gamma_0]E \\ &\quad +\gamma\exp(-\mathrm{i}\omega_0\tau)E(t-\tau), \\ \frac{\mathrm{d}N_1}{\mathrm{d}t} &= \frac{J}{e}-\frac{N_1}{T_1}-\Gamma_1\xi_1(N_1-N_{t1})|E|^2, \\ \frac{\mathrm{d}N_2}{\mathrm{d}t} &= -\frac{N_2}{T_2}-\Gamma_2\xi_2(N_2-N_{21})|E|^2, \end{aligned} \tag{17}$$

where E is the electric field and N_1 and N_2 are the electron densities for the active and absorbing regions (we refer the reader to [12] for a description of each of the physical constants). In the present study we ignore possible diffusion between the active and absorbing regions, nonlinear recombination effects so that T_j are constants, and we assume that the linewidth-enhancement factor α is equal in the active and absorbing media.

Introducing the new variables

$$\tilde{E}=\sqrt{\tau_1\Gamma_1\xi_1}E,\ D_j=\frac{\Gamma_j\xi_j}{\Gamma_0}(N_j-N_{tj})\ \text{ and } T=\Gamma_0 t \tag{18}$$

and constants

$$\begin{aligned}&\gamma_j=\frac{1}{T_j\Gamma_0},\ A_j=\frac{T_j\Gamma_j\xi_j}{\Gamma_0}\left(\delta_{j1}\frac{J}{e}-\frac{N_{tj}}{T_j}\right),\quad a=\frac{T_2\Gamma_2\xi_2}{T_1\Gamma_1\xi_1}, \\ &\eta=\frac{\gamma}{\Gamma_0},\qquad \tilde{\tau}=\Gamma_0\tau,\qquad\qquad \omega_\eta=\frac{\omega_0}{\Gamma_0}\end{aligned} \tag{19}$$

into equations (17), we obtain

$$\begin{aligned}\frac{\mathrm{d}\tilde{E}}{\mathrm{d}t} &= \frac{1}{2}[(1+\mathrm{i}\alpha)D_1+(1+\mathrm{i}\alpha)D_2-1]\tilde{E} \\ &\quad +\eta\exp(-\mathrm{i}\omega_\eta\tilde{\tau})\tilde{E}(t-\tilde{\tau}), \\ \frac{\mathrm{d}D_1}{\mathrm{d}t} &= \gamma_1[A_1-(1+|\tilde{E}|^2)D_1], \\ \frac{\mathrm{d}D_2}{\mathrm{d}t} &= \gamma_2[A_2-(1+a|\tilde{E}|^2)D_2]. \end{aligned} \tag{20}$$

Subsequently, we drop the tildes for notational convenience. Finally, we obtain (1) if we adiabatically ($\gamma_2 \gg \gamma_1$) eliminate D_2 and let $D = D_1$, $\gamma = \gamma_1$.

For the LSA without feedback, equation (1), rewritten in terms of the intensity $I = |E|^2$, has been studied in detail in [28] and was shown to possess many dynamical features of equation (20). Because of the additional complexity of obtaining both analytical and numerical results in the presence of feedback, we focus our analysis the simpler set of equations (1).

Appendix B: Hopf bifurcation conditions

Linear stability of the NZSS produces a characteristic equation for the eigenvalue λ; the delay results in a characteristic equation that is transcendental, having an infinite number of solutions. The Hopf-bifurcation point is found by setting $\lambda = \mathrm{i}\omega$ and simultaneously solving the real and imaginary parts of the characteristic equation. The two conditions are

$$\begin{aligned}&m_{22}[\eta^2(G_1^2-G_2^2)+2\eta\cos(\omega_\mathrm{s}\tau)G_2\omega-\omega^2] \\ &+\omega 2\eta G_1[\eta G_2-\omega\cos(\omega_\mathrm{s}\tau)]-\eta G_1 D(m_{12}m_{21}-m_{22}m_{11}) \\ &\qquad +\omega m_{11}(\eta G_2 D-\omega)=0\end{aligned}$$

$$\begin{aligned}&-\omega[\eta^2(G_1^2-G_2^2)+2\eta\cos(\omega_\mathrm{s}\tau)G_2\omega-\omega^2] \\ &\quad +m_{22}2\eta G_1[\eta G_2-\omega\cos(\omega_\mathrm{s}\tau)]-\omega m_{11}\eta G_1 \\ &\quad -(m_{12}m_{21}-m_{22}m_{11})(\eta G_2 D-\omega)=0\end{aligned} \tag{21}$$

where

$$\begin{aligned}&D=\cos(\omega_\mathrm{s}\tau)-\alpha\sin(\omega_\mathrm{s}\tau),\quad G_1=\cos(\omega\tau)-1, \\ &G_2=-\sin(\omega\tau),\qquad\qquad m_{11}=-\frac{aA_2F_\mathrm{s}^2}{(1+aF_\mathrm{s}^2)^2}, \\ &m_{12}=\frac{F_\mathrm{s}}{2},\qquad\qquad m_{21}=-\gamma\frac{2A_1F_\mathrm{s}}{(1+F_\mathrm{s}^2)}, \\ &m_{22}=-\gamma(1+F_\mathrm{s}^2),\qquad\qquad m_{31}=\frac{\alpha}{F_\mathrm{s}}m_{11}, \\ &m_{32}=\frac{\alpha}{2}.\end{aligned} \tag{22}$$

References

1. A.E. Siegman, *Lasers* (Univ. Science Books, 1986).
2. P. Mandel, *Theoretical Problems in Cavity Nonlinear Optics* (Cambridge Studies in Modern Optics, Cambridge University Press, New York, 1997).
3. G.P. Agrawal, N.K. Dutta, *Long-Wavelength Semiconductor Lasers* (Reinhold, New York, 1986).
4. M. Yamada, IEEE J. Quant. Electron. **29**, 1330 (1993).
5. D.R. Jones, P. Reese, I. Pierce, H.D. Summers, IEEE J. Select. Top. Quant. Electron. **5**, 740 (1999).
6. R. Lang, K. Kobayashi, IEEE J. Quant. Electron. **QE-16**, 347 (1980).
7. G.H.M. van Tartwijk, D. Lenstra, Quant. Semiclass. Opt. **7**, 87 (1995).

8. A. Gavrielides, T.C. Newell, V. Kovanis, R.G. Harrison, N. Swanston, Dejin Yu, Weiping Lu, Phys. Rev. A **60**, 1577 (1999).
9. S. Matsui, H. Takiguchi, H. Hayashi, S. Yamamoto, S. Yano, T. Hijikata, Appl. Phys. Lett. **43**, 219 (1983).
10. Y. Simler, J. Gamelin, S. Wang, IEEE Photon. Technol. Lett. **4**, 329 (1992).
11. E.A. Avrutin, Proc. Inst. Electr. Eng. **140**, 16 (1993).
12. G.H.M. van Tartwijk, M.S. Miguel, IEEE J. Quant. Electron. **32**, 1191 (1996).
13. T.W. Carr, T. Erneux, IEEE J. Quant. Electron. **37**, 1171 (2001).
14. T. Erneux, J. Opt. Soc. Am. B **5**, 1063 (1988).
15. A.M. Levine, G.H.M. van Tartwijk, D. Lenstra, T. Erneux, Phys. Rev. A **52**, R3436 (1995).
16. T. Erneux, Proc. SPIE **3944**, 588 (2000).
17. A. Ritter, H. Haug, J. Opt. Soc. Am. B **10**, 130 (1993).
18. D. Pieroux, T. Erneux, T. Luzyanina, K. Engelborghs, Phys. Rev. E **63**, 036211 (2001).
19. L.F. Shampine, S. Thompson, J. Appl. Numer. Math. **37**, 441 (2001); see also `http://www.cs.runet.edu/thompson/webddes/index.html`.
20. P.M. Alsing, V. Kovanis, A. Gavrielides, T. Erneux, Phys. Rev. A **53**, 4429 (1996).
21. A. Gavrielides, V. Kovanis, P.M. Varangis, T. Erneux, G. Lythe, Quant. Semiclass. Opt. **9**, 785 (1997).
22. P.M. Varangis, A. Gavrielides, T. Erneux, V. Kovanis, L.F. Lester, Phys. Rev. Lett. **78**, 2353 (1997).
23. G. Kozyreff, A.G. Vladimirov, P. Mandel, Phys. Rev. Lett. **85**, 3809 (2000).
24. T.W. Carr, D. Pieroux, P. Mandel, Phys. Rev. A **63**, 033817 (2001).
25. A.A. Tager, B.B. Elenkrig, IEEE J. Quant. Electron. **29**, 2886 (1993).
26. A.A. Tager, K. Peterrmann, IEEE J. Quant. Electron. **30**, 1553 (1994).
27. P. Peterson, A. Gavieledes, M.P. Sharma, T. Erneux, IEEE J. Quant. Electron. **35**, 1247 (1999).
28. W. Lauterborn, I. Eick, J. Opt. Soc. Am. B **5**, 1096 (1988).
29. E.J. Doedel, A.R. Champneys, T.F. Fairgrieve, Y.A. Kuznetsov, B. Sandstede, X. Wang, Auto97: Continuation and bifurcations software for ordinary differential equations (with homcont), `http://indy.cs.concordia.ca/auto`.